Frontiers of Information Technology & Electronic Engineering
www.jzus.zju.edu.cn; engineering.cae.cn; www.springerlink.com
ISSN 2095-9184 (print); ISSN 2095-9230 (online)
E-mail: jzus@zju.edu.cn

Model-free adaptive control for three-degree-of-freedom hybrid magnetic bearings*

Ye YUAN[1], Yu-kun SUN[†‡2], Qian-wen XIANG[1], Yong-hong HUANG[1], Zhi-ying ZHU[2]

([1]*School of Electrical and Information Engineering, Jiangsu University, Zhenjiang 212013, China*)

([2]*College of Electrical Engineering, Nanjing Institute of Technology, Nanjing 211167, China*)

[†]E-mail: sykujs421@163.com

Received May 21, 2017; Revision accepted July 13, 2017; Crosschecked Dec. 20, 2017

Abstract: Mathematical models are disappointing due to uneven distribution of the air gap magnetic field and significant unmodeled dynamics in magnetic bearing systems. The effectiveness of control deteriorates based on an inaccurate mathematical model, creating slow response speed and high jitter. To solve these problems, a model-free adaptive control (MFAC) scheme is proposed for a three-degree-of-freedom hybrid magnetic bearing (3-DoF HMB) control system. The scheme for 3-DoF HMB depends only on the control current and the objective balanced position, and it does not involve any model information. The design process of a parameter estimation algorithm is model-free, based directly on pseudo-partial-derivative (PPD) derived online from the input and output data information. The rotor start-of-suspension position of the HMB is regulated by auxiliary bearings with different inner diameters, and two kinds of operation situations (linear and nonlinear areas) are present to analyze the validity of MFAC in detail. Both simulations and experiments demonstrate that the proposed MFAC scheme handles the 3-DoF HMB control system with start-of-suspension response speed, smaller steady state error, and higher stability.

Key words: Model-free adaptive control; Hybrid magnetic bearings; Nonlinear areas; Faster response; Higher stability
https://doi.org/10.1631/FITEE.1700324 **CLC number:** TP273

1 Introduction

Climate change, as a result of global warming, is a critical problem in relation to the future of humanity. Greenhouse gas emissions, especially of CO_2, must soon be reduced to prevent the gradual increase of atmospheric concentrations to unacceptable levels. In this context, renewable energy technologies (O'Sullivan and Lewis, 2011; Sarkar and Ajjarapu, 2011; Casella, 2004) must be adapted, including water, wave, wind, solar, and geothermal power, to change the ongoing accelerating electrification trend. However, the supply of renewable energy is unstable. Electricity production depends on time, season, and temperature, among other factors. Therefore, a high-efficiency, non-polluting energy storage system should be established as a stable source of power supply.

The flywheel energy storage system (FESS) consists of a rotating device that stores kinetic energy in the form of rotational energy, via application of torque to its rotation axis (Lee *et al*., 2011; Zhang and Tseng, 2007; Subkhan and Komori, 2011). FESS is probably the most ancient way of storing energy, and modern developments (of magnetic bearings, effective power electronics, etc.) allow it to achieve performances suitable for electricity storage (Cimuca *et al.*, 2010; Wei *et al*., 2010). It is well known for its rapid charging and discharging. Furthermore, its life cycle is longer than that of batteries. Following years of development, FESS has been successfully applied

‡ Corresponding author

* Project supported by the National Natural Science Foundation of China (Nos. 51707082 and 51607080), the Natural Science Foundation of Jiangsu Province, China (Nos. BK20170546 and BK20150510), the China Postdoctoral Science Foundation (No. 2017M620192), and the Priority Academic Program Development of Jiangsu Higher Education Institutions

in satellites, dynamic uninterruptible power supplies, railway systems, etc..

However, FESS is usually limited by the costs associated with the rotor material, motors, and unit building. Furthermore, a FESS with a single flywheel unit cannot reach the required energy levels. Bearingless switched reluctance motors (BSRMs) (Morrison *et al*., 2008, Yang G *et al*., 2008; Cao and Deng, 2010; Yang Y *et al*., 2010; Chen and Hofmann, 2012) which are highly reliable, robust, fault tolerant, efficient, and compact, can be applied in FESSs with high temperatures or extreme temperature variations. The structure of the magnetic bearing (MB) is similar to that of the switched reluctance motor (SRM) stator; thus, bearingless technology is applied to the SRM to maximize its high-speed performance. BSRMs can not only rotate, but also achieve two-degree-of-freedom (2-DoF) levitation by integrating magnetic levitation windings into the motor stator. To reduce friction drag, FESSs are usually installed in a vacuum chamber. Nonetheless, this setup induces cooling problems due to conventional mechanical bearings.

An active 3-DoF MB with several advantages, such as elimination of a lubrication system, friction-free operation, and low power consumption, can be promoted in various practical industrial applications, especially in flywheel batteries. Most relevant studies have aimed at reducing the steady-state fluctuations and increasing the unbalanced response speed (Chen and Weng, 2010; Fang *et al*., 2010; Kang *et al*., 2010). Fang *et al*. (2010) discussed feedback linearization with a linear-state feedback controller and an integral sliding mode controller. Kang *et al*. (2010) applied a sliding mode control to increase the robustness of a 2-DoF MB control system and to reduce disturbance responses. For a voltage-controlled three-pole active MB system, a robust controller design is a nontrivial task because it is not a strict feedback form, as indicated by Chen and Weng (2010). Through a backstepping procedure, two stages of integral sliding-mode control are integrated to form a robust controller, and robust stabilization of a voltage-controlled three-pole MB system is considered. However, the MB suffers from significant power loss without a bias magnetic field compared with the hybrid magnetic bearing (HMB) (Han *et al*., 2013; Wang *et al*., 2014). In the current study, a permanent magnet biased magnetic bearing (PMBMB) is applied as a 3-DoF HMB. This bearing can produce biased magnetic fields with less winding action than what active magnetic bearings require. Thus, PMBMB and BSRM can realize 5-DoF levitation.

It is feasible to build a 3-DoF HMB control system with a model-based controller (MBC) or a data-driven controller (DDC). For MBC methods, the theoretical model of the plant should be built first, and the model parameters should be identified through rigorous mathematical methods. Then, the controller design is based on the identified acceptable model, which often requires much effort and time and can influence the performance of the control system. However, with the development of chemical industry, mechanical manufacturing, electronics, electrical, industrial and transportation industry, the system models are becoming more and more complex. Consequently, the effectiveness of MBC may become questionable without an acceptable model.

Recently, many plant DDCs have been developed, such as proportional-integral-derivative (PID) control (Formentin *et al*., 2012), iterative feedback tuning (Wakitani and Yamamoto, 2014), virtual reference feedback tuning (Hildebrand *et al*., 2005), and correlation-based tuning (Sala and Esparza, 2005). Because only the input/output (I/O) measurement data are used in the data-driven controller design procedure, the modeling process, unmodeled dynamics, and theoretical assumptions have less influence on control results, and DDCs have therefore caught considerable attention in recent years. However, most of them assume that the structure of the candidate controller is given a priori, and focus on the parameter-tuning algorithms. However, it is difficult to determine the structure of the candidate controller when the plant model is unavailable.

Model-free adaptive control (MFAC) (Mišković *et al*., 2007; Xu and Hou, 2009) can realize parameter adaptive control and structure adaptive control without the control object and control system model information. MFAC has the following advantages: (1) The MFAC design depends only on the input and output data information, which means that for actual industrial engineering, a universal controller can be designed. (2) Different from nonlinear adaptive control of a neural network, MFAC is a low-cost controller because a test signal and the training process are not necessary. (3) MFAC has the potential for use in practical applications due to the low computation cost, simple algorithm, and strong robustness. In this

study, we propose MFAC for an HMB control system that consists of a control algorithm, a parameter estimation algorithm, and a parameter reset algorithm. The simulation and experiment results indicate that the MB control system with the MFAC controller has better performance than with a PID controller.

2 Configuration and operation principle

A key technology of FESS is its support mechanism. This technique not only stabilizes flywheel operation but also reduces the size of the flywheel rotor. Currently, the supporting parts are mechanical, including a superconducting magnetic bearing, an electromagnetic suspension, and a permanent magnetic bearing (PMB). FESS consists mainly of a bearingless motor, a 3-DoF HMB, and a PMB. Specifically, the single winding bearingless flywheel motor (SWBFM) (Zhu and Hou, 2015) used is an improvement on the BSRM structure. PMBMB is adopted as a 3-DoF HMB, and a PMB is employed in unloading.

Fig. 1 shows a schematic of the 3-DoF HMB for FESS. The configuration of FESS with an SWBFM, a 3-DoF HMB, and a PMB is shown in Fig. 1a. The configuration of a 3-DoF HMB (axial control coils are hidden in active view) is shown in Fig. 1b and its exploded view is shown in Fig. 1c (axial control coils and radial control coils are hidden in active view). The 3-DoF HMB is made up of a radial stator with four poles, four radial control coils, a rotor lamination, an axial stator with two radial control coils, and an axial magnetized permanent magnet.

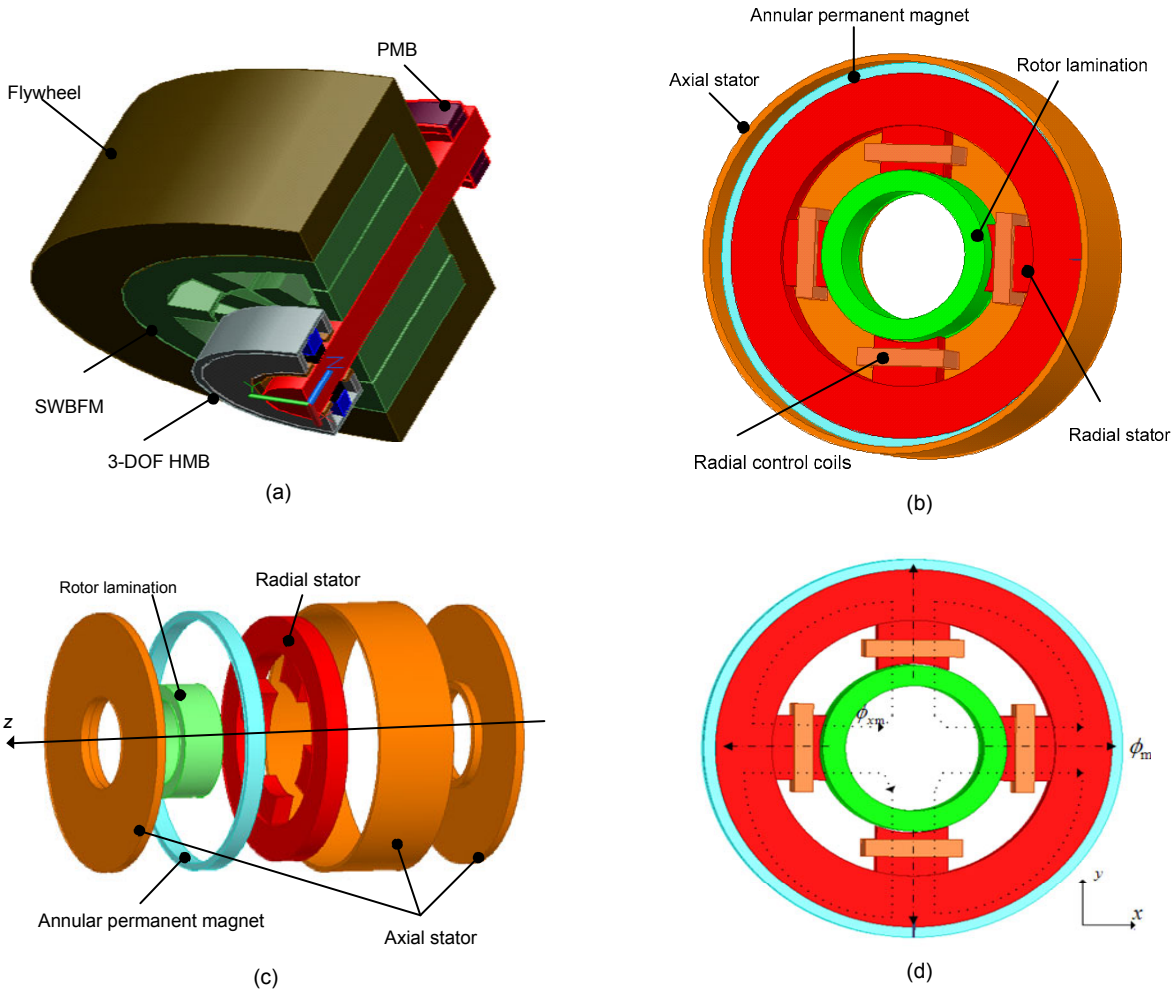

Fig. 1 Schematic of 3-DoF HMB for FESS: (a) configuration of FESS; (b) configuration of 3-DoF HMB; (c) exploded view of 3-DoF HMB; (d) schematic of radial force

The 2-DoF radial forces and 1-DoF axial force can be produced by the 3-DoF HMB. The operation principle of radial force in the x-direction is presented in Fig. 1d. The ϕ_{xm} produced by radial control coils is the control magnetic flux in the x-direction and the ϕ_m is the bias magnetic flux produced by the permanent magnet.

Given the symmetrical structure of PMBMB, ϕ_m is a constant in the positive and negative x-direction. If the rotor is suspended in an equilibrium position, only the biased flux is generated by the permanent magnet circuits in magnetic bearing. The resultant force is zero. The flux density distribution without control current is shown in Fig. 2a. If the rotor is pushed in the negative x-direction by an external force, then the length of the air gap increases and the ϕ_{xm} decreases in the positive x-direction. The length of the air gap decreases when the ϕ_m increases in the negative x-direction. The control flux ϕ_{xm} will be added to the biased flux ϕ_m, and the resultant force generated by synthesized magnetic flux will suspend the rotor in an equilibrium position. The flux density distribution with maximum control current is shown in Fig. 2b. The structural parameters are presented in Table 1.

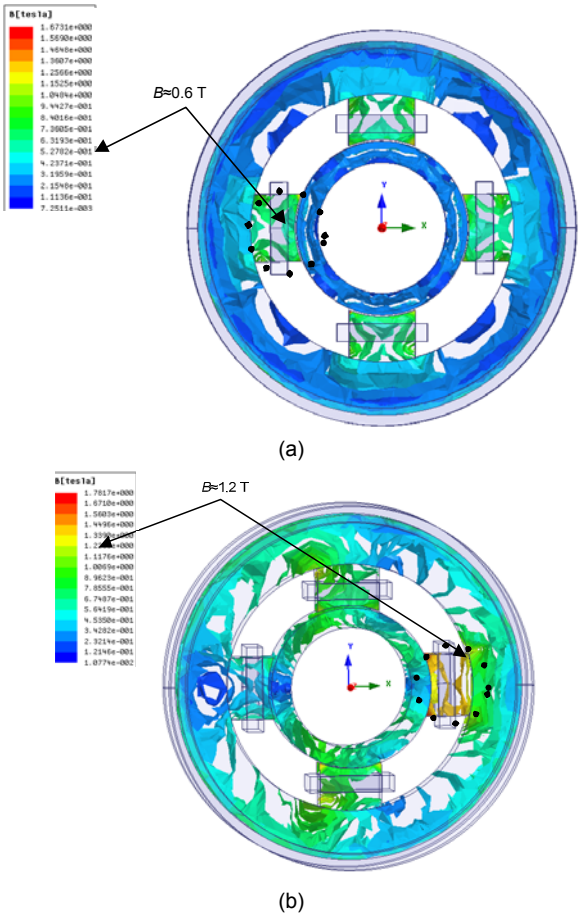

Fig. 2 Flux density distribution of radial stator and rotor lamination: (a) flux density distribution without control current; (b) flux density distribution with the maximum control current

Table 1 Prototype specification

Parameter	Value
Maximum axial force F_z	200 N
Maximum radial force F_{xy}	100 N
Outside diameter	130 mm
Inner diameter	37 mm
Permanent magnet thickness	3 mm
Rated current	4 A
Air gap length	0.5 mm
Magnetic flux density	1.2 T

3 Control system analysis of 3-DoF HMB

3.1 Compact form dynamic linearization model-free adaptive control

Consider a nonlinear controlled model:

$$y(k+1)=f(y(k),...,y(k-n_y),u(k),...,u(k-n_u)), \quad (1)$$

where $f(\cdot)$ is an unknown nonlinear function, $u(k)$ is the input variable, $y(k)$ is the output variable, k is the sampling instant, and n_y and n_u are the unknown control system orders. Compact form dynamic linearization (CFDL) can be obtained with the following reasonable assumptions:

Assumption 1 A bounded control input signal $u(k)$ makes system output equal to the bounded expected output (defined as $y^*(k+1)$).

Assumption 2 The partial derivative of $f(\cdot)$ with respect to $u(k)$ is continuous.

Assumption 3 System (1) is generalized Lipschitz; i.e., it satisfies $\Delta y(k+1)\le b|\Delta u(k)|$, $\forall k$ and $||\Delta u(k)||\neq 0$, where $\Delta y(k+1)=y(k+1)-y(k)$, $\Delta u(k)=u(k)-u(k-1)$, and b is a constant.

Theorem 1 For nonlinear system (1), we assume that Assumptions 1, 2, and 3 hold. When $||\Delta u(k)||\neq 0$, there must exist a parameter called the 'pseudo-partial derivative' (PDD, a time-varying parameter). System

(1) can be transformed into the following CFDL description:

$$\Delta y(k+1)=\phi(k)\left|\Delta u(k)\right|, \tag{2}$$

where $|\phi(k)|\leq C$ and C is a positive constant. If the values of k and $\Delta u(k)$ are very small, PDD is a slow-time-varying parameter.

To guarantee that the expression of the general nonlinear system (1) can be reasonably substituted by dynamic linearization (2), an adjustable weighting factor λ is adopted to keep the value of $\Delta u(k)$ in a small range and to reduce the steady-state tracking error. To obtain the optimal controller parameters, the criterion function is as follows:

$$J(u(k))=\left|y^*(k+1)-y(k+1)\right|^2+\lambda\left|u(k)-u(k-1)\right|^2, \tag{3}$$

where $y^*(k+1)$ is the desired system output.

From Eqs. (2) and (3), the partial derivate of J with respect to controller parameters $u(k)$ can be obtained easily as

$$\begin{aligned}\frac{\partial J(u(k))}{\partial u(k)}&=2(y^*(k+1)-y(k))\phi(k)\\&\quad-\left|\phi(k)\right|^2(u(k)-u(k-1))\\&\quad+2\lambda(u(k)-u(k-1)).\end{aligned} \tag{4}$$

Obviously, optimal controller parameters $u(k)$ can be calculated analytically by setting expression (4) to be zero if the plant model is available, i.e.,

$$u(k)=u(k-1)+\frac{\rho\phi(k)}{\lambda+\left|\phi(k)\right|^2}(y^*(k+1)-y(k)), \tag{5}$$

where ρ ($\rho\in(0, 1]$) is a step length factor that can make the control system universal. It can be easily determined from Eq. (5) that only the input/output (I/O) measurement data are used in the data-driven controller design procedure, and that the modeling process, the unmodeled dynamics, and the theoretical assumptions are omitted.

Generally, the estimation algorithms based on the traditional parameter estimation criterion function cause the values of estimated parameters to change too fast or cause the control system to be sensitive to the mutation sampling data.

Thus, a new parameter estimation criterion function can be written as

$$\begin{aligned}J(\phi(k))&=\left|y(k)-y(k-1)-\phi(k)\Delta u(k-1)\right|^2\\&\quad+u\left|\phi(k)-\hat{\phi}(k-1)\right|^2,\end{aligned} \tag{6}$$

where μ is the penalty factor.

According to the extreme value of expression (6), the PPD estimation algorithm is as follows:

$$\begin{aligned}\phi(k)&=\hat{\phi}(k-1)+\frac{\eta\Delta u(k-1)}{\mu+\Delta u(k-1)^2}\\&\quad\cdot(\Delta y(k)-\hat{\phi}(k-1)\Delta u(k-1))^2,\end{aligned} \tag{7}$$

where η is the step factor and $\hat{\phi}(k)$ is the estimated value of $\phi(k)$.

In the conditions $\hat{\phi}(k)\leq\varepsilon$, $\Delta u(k-1)\leq\varepsilon$, or $\operatorname{sign}(\hat{\phi}(k))\neq\operatorname{sign}(\hat{\phi}(1))$, the reset algorithm CFDL-MFAC can be written as

$$\hat{\phi}(k)=\hat{\phi}(1), \tag{8}$$

where ε is a positive number with a very small value and $\hat{\phi}(1)$ is the initial value of $\hat{\phi}(k)$.

3.2 Control system of 3-DoF HMB

In this study, the experimental 3-DoF HMB system is designed according to the specification presented in Table 1. The general description of the x-position control system of 3-DoF HMB is presented in a basic control chart using algorithms (Fig. 3). In this system, x^*, y^*, and z^* are the desired system outputs, i.e., the balanced position, and its value usually equals zero, especially in the MB controller system. The position deviation signals in the radial and axial directions, which are fed into the controllers, can be obtained by the displacement sensor in the x-, y-, and z-direction. The control current reference signals are produced by the current converter, which receives the output signals from the controllers (F_x, F_y, F_z).

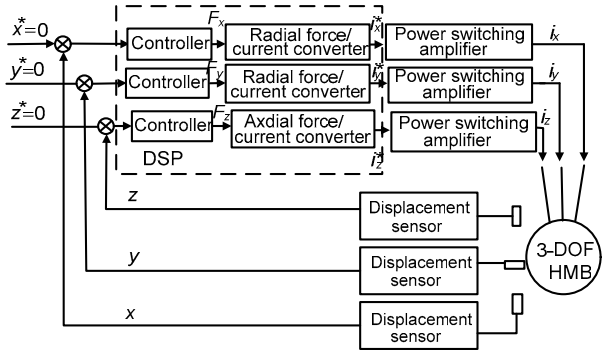

Fig. 3 A basic control chart of 3-DoF hybrid magnetic bearing (HMB)

The relationships among radial control current i_x, displacement in the x-direction, and radial levitation force F_x are exhibited in Fig. 4. The rotor is at the balanced position in the z- and y-direction, and the value of the control current in the z- and y-direction is zero.

When the radial displacement in the x-direction fluctuates at [−0.2, 0.2] mm, the graph tilts at a certain angle along the x-y plane. This finding in Fig. 4a indicates that the radial levitation force is proportional to radial displacement x. Similarly, the radial levitation force F_x is proportional to radial control current i_x. However, when the radial displacement in the x-direction fluctuates at [−0.4, −0.2] mm and [0.2, 0.4] mm, the corresponding areas are nonlinear, and are generated according to magnetic saturation with the fluctuation of the radial displacement as the air gap shortens.

The relationship between radial displacement x and radial levitation force F_x is shown in Fig. 4b. When the radial displacement in the x-direction fluctuates at [−0.2, 0.2] mm, the radial levitation force F_x is proportional to x. When the radial displacement in the x-direction fluctuates at [−0.2, −0.4] mm and [0.2, 0.4] mm, the relationship between x and F_x is nonlinear.

The relationship between radial control current i_x and radial levitation force F_x is shown in Fig. 4c. When the radial displacement in the x-direction fluctuates at [−2, 2] A, F_x is proportional to radial control current i_x. When the radial displacement in the x-direction fluctuates at [−4, −2] A and at [2, 4] A, the relationship between i_x and F_x is nonlinear.

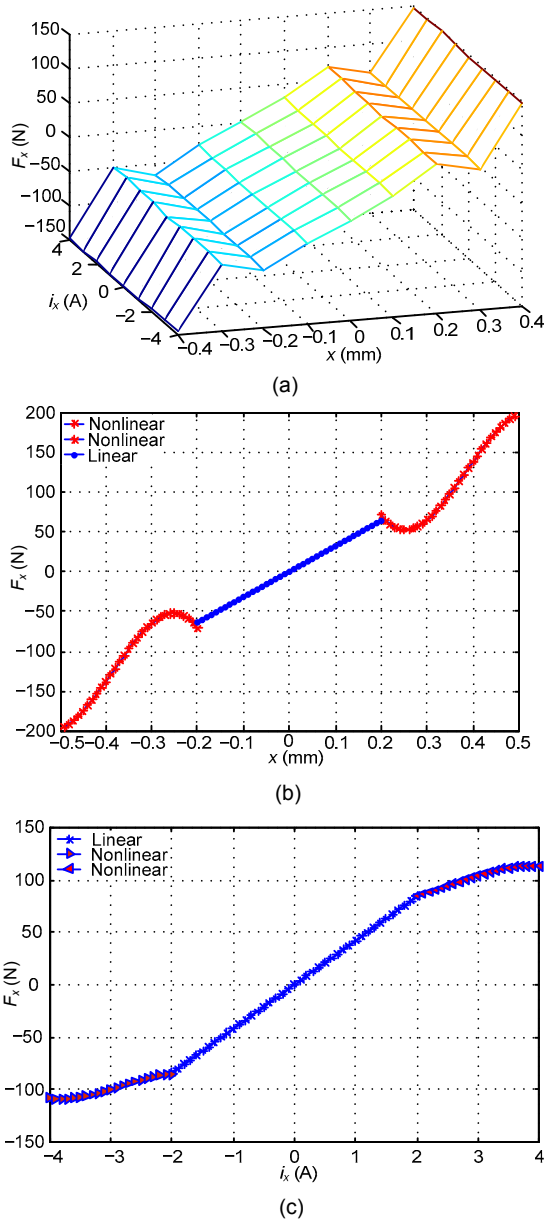

Fig. 4 Relationship among i_x, x, and F_x (a), relationship between x and F_x (b), and relationship between i_x and F_x (c)

4 Simulation and experiments

Based on the above analysis, it is obvious that the linear control system for the linear region and the nonlinear control system for the nonlinear region should be studied independently to verify the validity of MFAC. The control system of 3-DoF HMB consists of three subsystems: the subsystem in the

x-direction, the subsystem in the y-direction, and the subsystem in the z-direction. Considering the similarity of subsystems according to the symmetric physical structure of the HMB, only the subsystem in the x-direction is analyzed.

The mathematical model in the x-direction is written as

$$F_x = k_1 i_x - k_2 x, \tag{9}$$

where k_1 is the current stiffness coefficient and k_2 is the displacement stiffness coefficient. In this study, the value of k_1 is 42 N/A and the value of k_2 is 300 N/mm. The force/current converter in the x-direction can be realized based on Eq. (9).

4.1 Start-of-suspension of simulation results in the linear system

Under normal circumstances, the HMB operates in the linear area with the backup bearing, and the inner diameter of the backup bearing is 0.2 mm. The linear control system of 3-DoF HMB in the x-direction in Fig. 3 is controlled with a PID or MFAC. For a PID controller, a differential restriction link and integral separation are applied in the control system. The transfer function of this controller is obtained as follows:

$$G(s) = \begin{cases} \dfrac{K_\mathrm{p}(1+T_\mathrm{d}S)}{1+\tau T_\mathrm{d}S}\left(1+\dfrac{1}{T_\mathrm{i}S}\right), & |e| \le c, \\ \dfrac{K_\mathrm{p}(1+T_\mathrm{d}S)}{1+\tau T_\mathrm{d}S}, & |e| > c, \end{cases} \tag{10}$$

where K_p is the proportionality coefficient, T_i is the integral action time constant, T_d is the derivative action time constant, τ is the differential gain coefficient, e is the difference between the equilibrium position reference signals and position feedback signals, and c is the threshold value.

The algorithm parameters of MFAC and the PID in the linear system are shown in Table 2.

Table 2 Algorithm parameters

Model-free adaptive control	PID-linear
$\hat{\phi}(1)$ =2	K_p=11
ρ=0.01	T_i=0.008
η=1.5	T_d=0.01
μ=1.5	τ=0.05
ε=0.0005	

With other PID parameters, the response speed would be slower or overshoot would be higher; i.e., fast response and low overshoot are the principle of choosing the parameters.

The simulation results of displacement responses in the x-direction are presented in Fig. 5.

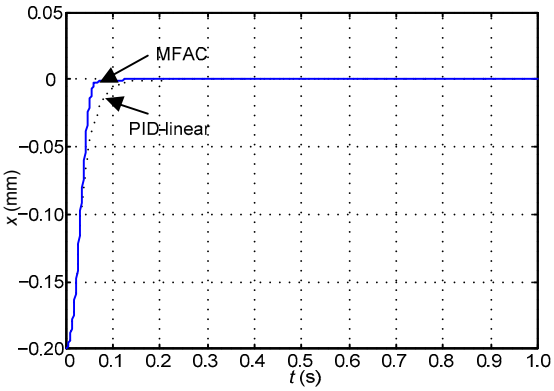

Fig. 5 Displacement responses in the linear area

The rotor starts at a stationary position when the system is turned on, and the initial coordinates are x=−0.2 mm, y=0 mm, and z=0 mm (Fig. 5). The rotor is successfully suspended in the balanced position from the initial position −0.2 mm. For PID control, the rotor returns to the balanced position within 150 ms. For MFAC, the rotor returns to the balanced position within 100 ms and the response time is reduced by about 33% compared with PID control. This behavior indicates that the HMB control system with MFAC has higher response speed in the linear area.

4.2 Start-of-suspension simulation results in a nonlinear system

FESS can be used in extreme environments, such as on a drone, on warships, and on satellites. The air gap length of the backup bearing is expanded to a nonlinear area; i.e., it is difficult to obtain the mathematical model in a nonlinear area or the mathematical model is not accurate.

In this study, we use the least squares support vector machine (LS-SVM) (Yuan *et al*., 2015) instead of a mathematical model and the control system (Fig. 6a). The algorithm parameters of MFAC, the linear PID system, and the nonlinear PID system are shown in Table 3. The simulation results of displacement responses in the x-direction are presented in Fig. 6b.

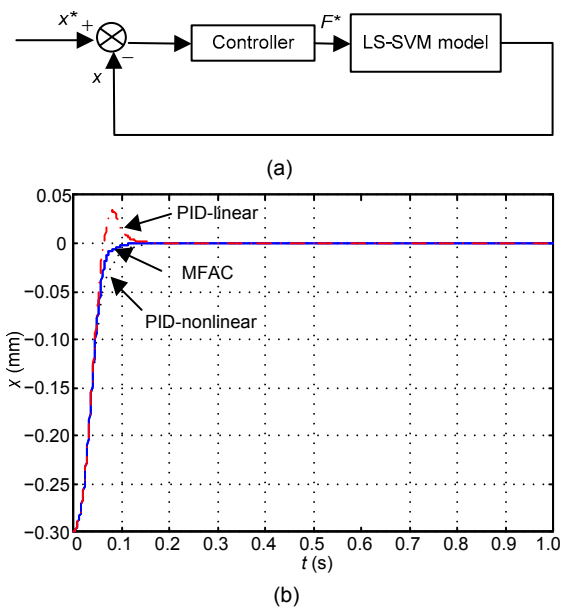

Fig. 6 Study on nonlinear area control: (a) nonlinear control system of 3-DoF HMB in the *x* position; (b) displacement responses in the nonlinear area

Table 3 Algorithm parameters

MFAC	PID-linear	PID-nonlinear
$\hat{\phi}(1)$ =2	K_p=11	K_p=11
ρ=0.01	K_i=0.008	K_i=0.012
η=1.5	K_d=0.0095	K_d=0.0012
μ=1.5	τ=0.05	τ=0.05
ε=0.0005		

Similar to start-of-suspension in the linear area, Fig. 6b shows that in three cases, the rotor is successfully suspended in the balanced position from the initial position −0.3 mm. For PID-linear control, the rotor returns to the balanced position within 180 ms, but the overshoot of eccentric adjustment is obviously about 0.04 mm. This means that the PID parameters in the linear system should be adjusted to fit the nonlinear system. Thus, with the adjusted nonlinear PID parameters, the rotor returns to the balanced position within 140 ms and the outshoot is eliminated. For MFAC, the rotor returns to the balanced position within 110 ms and the overshoot is reduced by about 100% compared with linear PID. The response time is reduced by about 25% compared with nonlinear PID. That is, if the linear PID parameters are used in a nonlinear system, the control result is unsatisfactory and the PID parameters should be reset. However, regardless of whether the HMB operates in the linear area or nonlinear area, the control result is satisfactory. This behavior indicates that MFAC has better system adaptability and faster response speed.

4.3 Experimental results

A complete rotor model contains six degrees of freedom. The axial rotation driven by a motor provides a freedom. The HMB presented in this study serves the rotor model system in charge of one axial DoF and two radial 2-DoFs. An SWBFM is in charge of the other two DoFs of the rotor model. In addition, backup bearings are installed around the shaft and the rotor system is regarded as five single-DoF systems. In this study, we take the rotor dynamics in the *x*-direction of the radial axis as an example to demonstrate the performance of the proposed control method.

The control algorithm is implemented in a TMS320F2812 DSP. A self-researched TMS320F2812 DSP basic board based on the chip was designed that enables the digital control system to satisfy the requirements for stable operation. The input voltage range of the analog-to-digital converter in the DSP board is 0−3 V, but the output voltage range of the displacement sensor is −18 to −2 V. Thus, the displacement signal detected by the displacement sensor cannot be directly transferred to the DSP board, and the displacement interface circuit must be added to adjust unmatched voltage.

4.3.1 Experimental results of start-of-suspension

Fig. 7 shows the experimental results of the start of suspension of the HMB linear control system using the MFAC and linear PID parameters are shown in Fig. 7. The rotor suspends from the initial stationary coordinates (−0.2, 0, 0) mm to the balanced coordinates (0, 0, 0) mm.

Fig. 7a shows that it takes about 150 ms for start-of-suspension. Fig. 7b shows that it takes about 100 ms for start-of-suspension. After the rotor reaches the equilibrium position, the rotor remains stable with some steady-state errors. Comparing Figs. 7a and 7b, it is obvious that in an actual linear control system, the response speed of start-of-suspension is faster with MFAC.

The experimental results of the start-of-suspension of the HMB nonlinear control system using MFAC and nonlinear PID parameters are shown

in Fig. 8. The rotor suspends from the initial stationary coordinates (−0.3, 0, 0) mm to the balanced coordinates (0, 0, 0) mm.

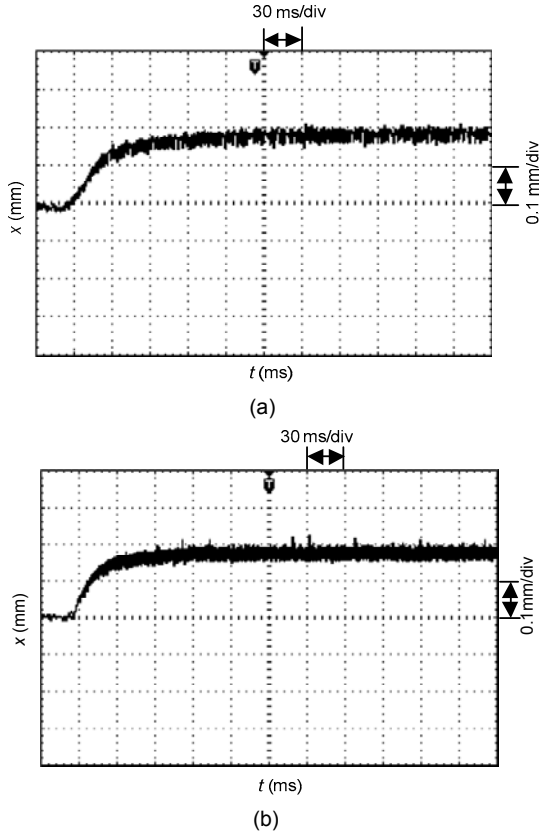

Fig. 7 Start-of-suspension waveform of HMB in the linear area: (a) start-of-suspension waveform with PID; (b) start-of-suspension waveform with MFAC

It takes about 140 ms for start-of-suspension with PID control in Fig. 8a, and the waveform matches the simulation results in about 120 ms for start-of-suspension with MFAC in Fig. 8b. The waveforms match the simulation results shown in Fig. 6b. After the rotor reaches the equilibrium position, it remains stable with some steady-state errors. Comparing Figs. 8a and 8b, it is obvious that in an actual nonlinear control system, the response speed of start-of-suspension is faster based on MFAC.

4.3.2 Experimental results of stable suspension

The above analysis is focused on the start-of-suspension; in this subsection, displacement waveforms of stable suspension at a shaft speed (defined as n) of 6000 r/min in the x- and y-direction is presented.

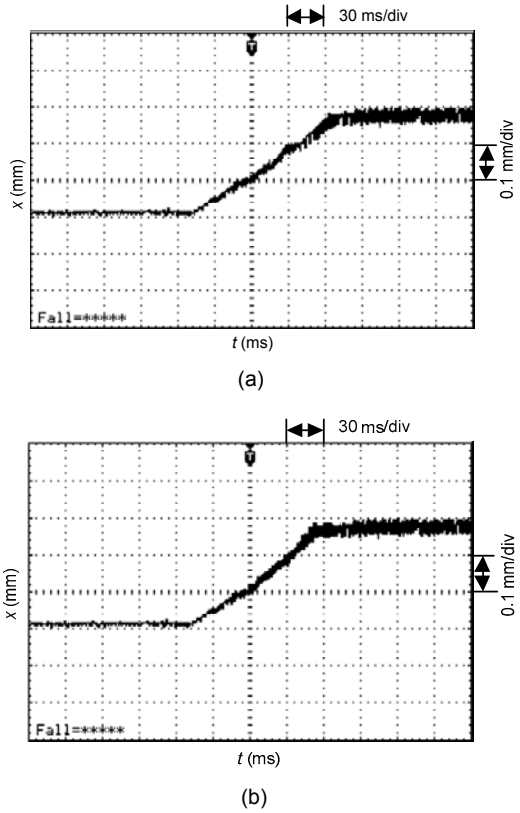

Fig. 8 Start-of-suspension waveform of HMB in the nonlinear area: (a) start-of-suspension waveform with PID; (b) start-of-suspension waveform with MFAC

Fig. 9a illustrates the displacement waveforms at n=6000 r/min in the x- and y-direction with a PID controller. When the rotor is in stable suspension, the fluctuation of unilateral displacement in the y-direction is about 80 μm, or 16% of the length of the air gap (0.5 mm). Moreover, the unilateral displacement fluctuation in the x-direction is roughly 50 μm, or 10% of the length of the air gap. The displacement fluctuation is far less than the length of the air gap.

Fig. 9b illustrates the displacement waveforms at n=6000 r/min in the x- and y-direction with MFAC. When the rotor is in stable suspension, the fluctuation of unilateral displacement in the y-direction is about 60 μm, or 12% of the length of the air gap. Moreover, the unilateral displacement fluctuation in the x-direction is roughly 30 μm, or 6% of the length of the air gap. The displacement fluctuation is far less than the length of the air gap. In addition, due to the weight of the shaft, the fluctuation of unilateral displacement in the y-direction is higher than the displacement in the x-direction.

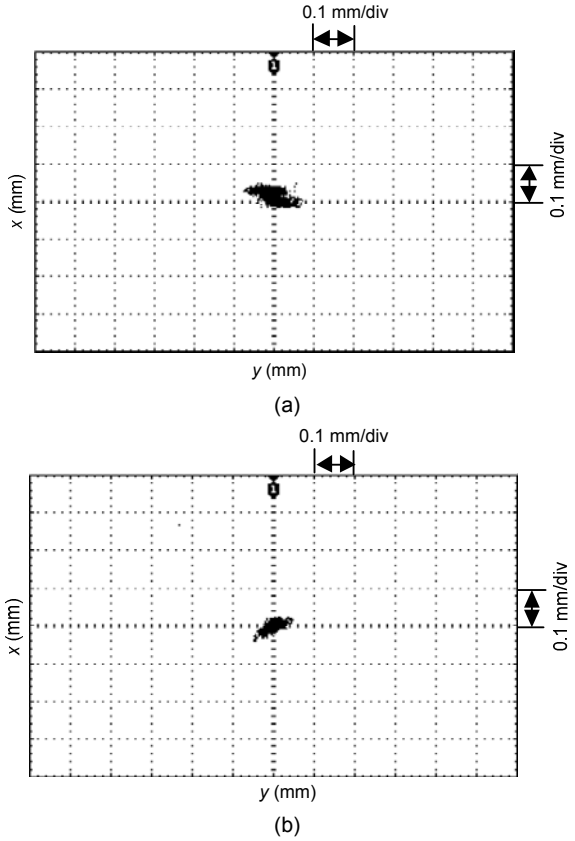

Fig. 9 Stable suspension waveforms at n=6000 r/min: (a) displacement waveforms with the PID controller; (b) displacement waveforms with MFAC

Comparing Figs. 9b with 9a, it is obvious that in an actual nonlinear control system, the steady-state error is smaller and the stability is higher based on MFAC.

5 Conclusions

A 3-DoF HMB used for FESS has been considered in this paper. To strengthen the stability, response speed, and robustness of the HMB control system, an MFAC scheme is applied, which depends only on I/O data from the plant and consists of a control algorithm, a parameter estimation algorithm, and a parameter reset algorithm. To analyze the validity of MFAC in detail, the working environment of start-of-suspension is divided into two situations, linear and nonlinear areas; i.e., the extreme condition is considered. For the start-of-suspension in linear areas, the response speed with MFAC is 50 ms faster than with PID control; in nonlinear areas, the response speed with MFAC is 20 ms faster than with PID control. Moreover, in the stable suspension stage, the experiments demonstrate that the proposed 3-DoF HMB MFAC handles dynamic rotor control with a smaller steady-state error and higher stability. This design procedure, with its low computation cost and simple algorithm structure, has the potential for practical applications.

References

Cao, X., Deng, Z.Q., 2010. A full-period generating mode for bearingless switched reluctance generators. *IEEE Trans. Appl. Supercond.*, **20**(3):1072-1076. https://doi.org/10.1109/TASC.2010.2041206

Casella, F., 2004. Modeling, simulation, control, and optimization of a geothermal power plant. *IEEE Trans. Energy Conv.*, **19**(1):170-178. https://doi.org/10.1109/TEC.2003.821823

Chen, L., Hofmann, W., 2012. Speed regulation technique of one bearingless 8/6 switched reluctance motor with simpler single winding structure. *IEEE Trans. Ind. Electron.*, **59**(6):2592-2600. https://doi.org/10.1109/TIE.2011.2163289

Chen, S.L., Weng, C.C., 2010. Robust control of a voltage-controlled three-pole active magnetic bearing system. *IEEE/ASME Trans. Mechatron.*, **15**(3):381-388. https://doi.org/10.1109/TMECH.2009.2027015

Cimuca, G., Breban, S., Radulescu, M.M., *et al*., 2010. Design and control strategies of an induction-machine-based flywheel energy storage system associated to a variable-speed wind generator. *IEEE Trans. Energy Conv.*, **25**(2): 526-534. https://doi.org/10.1109/TEC.2010.2045925

Fang, J.C., Sun, J.J., Liu, H., *et al*., 2010. A novel 3-DoF axial hybrid magnetic bearing. *IEEE Trans. Magn.*, **46**(12): 4034-4045. https://doi.org/10.1109/TMAG.2010.2074206

Formentin, S., Savaresi, S.M., Del Re, L., 2012. Non-iterative direct data-driven controller tuning for multivariable systems: theory and application. *IET Contr. Theory Appl.*, **6**(9):1250-1257. https://doi.org/10.1049/iet-cta.2011.0204

Han, B.C., Zheng, S.Q., Le, Y., *et al*., 2013. Modeling and analysis of coupling performance between passive magnetic bearing and hybrid magnetic radial bearing for magnetically suspended flywheel. *IEEE Trans. Magn.*, **49**(10):5356-5370. https://doi.org/10.1109/TMAG.2013.2263284

Hildebrand, R., Lecchini, A., Solari, G., *et al*., 2005. Asymptotic accuracy of iterative feedback tuning. *IEEE Trans. Autom. Contr.*, **50**(8):1182-1185. https://doi.org/10.1109/TAC.2005.852551

Kang, M.S., Lyou, J., Lee, J.K., 2010. Sliding mode control for an active magnetic bearing system subject to base motion. *Mechatronics*, **20**(1):171-178.

https://doi.org/10.1016/j.mechatronics.2009.09.010

Lee, J., Jeong, S., Han, Y.H., *et al*., 2011. Concept of cold energy storage for superconducting flywheel energy storage system. *IEEE Trans*. *Appl*. *Supercond*., **21**(3): 2221-2224. https://doi.org/10.1109/TASC.2010.2094177

Mišković, L., Karimi, A., Bonvin, D., *et al*., 2007. Correlation-based tuning of decoupling multivariable controllers. *Automatica*, **43**(9):1481-1494. https://doi.org/10.1016/j.automatica.2007.02.006

Morrison, C.R., Siebert, M.W., Ho, E.J., 2008. Electromagnetic forces in a hybrid magnetic-bearing switched-reluctance motor. *IEEE Trans*. *Magn*., **44**(12):4626-4638. https://doi.org/10.1109/TMAG.2008.2002891

O'Sullivan, D.L., Lewis, A.W., 2011. Generator selection and comparative performance in offshore oscillating water column ocean wave energy converters. *IEEE Trans*. *Energy Conv*., **26**(2):603-614. https://doi.org/10.1109/TEC.2010.2093527

Sala, A., Esparza, A., 2005. Extensions to "virtual reference feedback tuning: a direct method for the design of feedback controllers". *Automatica*, **41**(8):1473-1476. https://doi.org/10.1016/j.automatica.2005.02.008

Sarkar, S., Ajjarapu, V., 2011. MW resource assessment model for a hybrid energy conversion system with wind and solar resources. *IEEE Trans*. *Sustain*. *Energy*, **2**(4):383-391. https://doi.org/10.1109/TSTE.2011.2148182

Subkhan, M., Komori, M., 2011. New concept for flywheel energy storage system using SMB and PMB. *IEEE Trans*. *Appl*. *Supercond*., **21**(3):1485-1488. https://doi.org/10.1109/TASC.2010.2098470

Wakitani, S., Yamamoto, T., 2014. Design and application of a data-driven PID controller. Proc. IEEE Conf. on Control Applications, p.1443-1448. https://doi.org/10.1109/CCA.2014.6981527

Wang, K., Wang, D., Lin, H.Y., *et al*., 2014. Analytical modeling of permanent magnet biased axial magnetic bearing with multiple air gaps. *IEEE Trans*. *Magn*., **50**(11):1-4. https://doi.org/10.1109/TMAG.2014.2330843

Wei, K.Y., Liu, D.Z., Meng, J., *et al*., 2010. Design and simulation of a 12-phase flywheel energy storage generator system with linearly dynamic load. *IEEE Trans*. *Appl*. *Supercond*., **20**(3):1050-1054. https://doi.org/10.1109/TASC.2010.2040599

Xu, J.X., Hou, Z.S., 2009. Notes on data-driven system approaches. *Acta Autom*. *Sin*., **35**(6):668-675. https://doi.org/10.1016/S1874-1029(08)60090-7

Yang, G., Deng, Z.Q., Cao, X., *et al*., 2008. Optimal winding arrangements of a bearingless switched reluctance motor. *IEEE Trans*. *Power Electron*., **23**(6):3056-3066. https://doi.org/10.1109/TPEL.2008.2002070

Yang, Y., Deng, Z.Q., Yang, G., *et al*., 2010. A control strategy for bearingless switched-reluctance motors. *IEEE Trans*. *Power Electron*., **25**(11):2807-2819. https://doi.org/10.1109/TPEL.2010.2051684

Yuan, Y., Sun, Y.K., Huang, Y.H., *et al*., 2015. Harmony chaotic search optimal design of single winding bearingless switched reluctance flywheel motors. *Tran*. *China Electrotechn*. *Soc*., **30**(2):180-188 (in Chinese). https://doi.org/10.3969/j.issn.1000-6753.2015.02.024

Zhang, C., Tseng, K.J., 2007. A novel flywheel energy storage system with partially-self-bearing flywheel-rotor. *IEEE Trans*. *Energy Conv*., **22**(2):477-487. https://doi.org/10.1109/TEC.2005.858088

Zhu, Y.M., Hou, Z.S., 2015. Controller dynamic linearisation-based model-free adaptive control framework for a class of non-linear system. *IET Contr. Theory Appl*., **9**(7): 1162-1172. https://doi.org/10.1049/iet-cta.2014.0743